JACS
JOURNAL OF THE AMERICAN CHEMICAL SOCIETY
pubs.acs.org/JACS

Article

Autoinhibition in the Signal Transducer CIN85 Modulates B Cell Activation

Daniel Sieme, Michael Engelke, Nasrollah Rezaei-Ghaleh, Stefan Becker, Jürgen Wienands, and Christian Griesinger*

Cite This: https://doi.org/10.1021/jacs.3c09586

ABSTRACT: Signal transduction by the ligated B cell antigen receptor (BCR) depends on the preorganization of its intracellular components, such as the effector proteins SLP65 and CIN85 within phase-separated condensates. These liquid-like condensates are based on the interaction between three Src homology 3 (SH3) domains and the corresponding proline-rich recognition motifs (PRM) in CIN85 and SLP65, respectively. However, detailed information on the protein conformation and how it impacts the capability of SLP65/CIN85 condensates to orchestrate BCR signal transduction is still lacking. This study identifies a hitherto unknown intramolecular SH3:PRM interaction between the C-terminal SH3 domain (SH3C) of CIN85 and an adjacent PRM. We used high-resolution nuclear magnetic resonance (NMR) experiments to study the flexible linker region containing the PRM and determined the extent of the interaction in multidomain constructs of the protein. Moreover, we observed that the phosphorylation of a serine residue located in the immediate vicinity of the PRM regulates this intramolecular interaction. This allows for a dynamic modulation of CIN85's valency toward SLP65. B cell culture experiments further revealed that the PRM/SH3C interaction is crucial for maintaining the physiological level of SLP65/CIN85 condensate formation, activation-induced membrane recruitment of CIN85, and subsequent mobilization of Ca^{2+}. Our findings therefore suggest that the intramolecular interaction with the adjacent disordered linker is effective in modulating CIN85's valency both *in vitro* and *in vivo*. This therefore constitutes a powerful way for the modulation of SLP65/CIN85 condensate formation and subsequent B cell signaling processes within the cell.

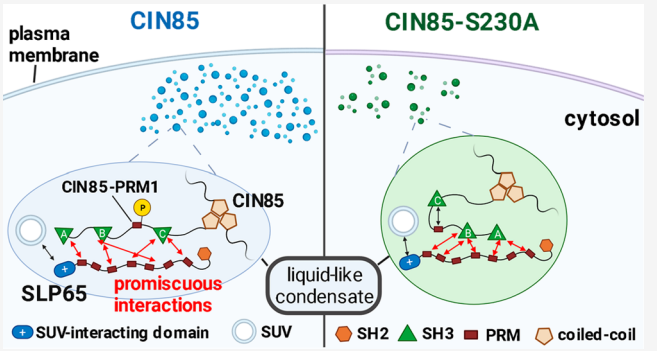

INTRODUCTION

Scaffold proteins play an important role in the spatial and temporal organization of cellular processes, and thus their significance for many of the interconnected signaling pathways cannot be overstated. Their efficient use of multiple modular domains and intrinsically disordered regions (IDR) enables the formation of the large macromolecular assemblies that play an important role in nearly all of the signaling pathways known within the cell.[1] Specific functions range from recruiting effectors to specific subcellular locations,[2] providing docking sites for the assembly of higher-order macromolecular structures[3,4] and to fine-tune the often weak and transient interactions within these assemblies.[5] In particular, the combination of modular folded domains connected via IDR leads to multidomain proteins with a large potential for internal dynamics, necessary for their many different functions. Consistently, the same scaffold protein can play different roles in separate signaling pathways, depending on differential splicing, post-translational modifications (PTM), and/or the presence of different other effector and scaffold proteins.[6]

The Cbl-interacting protein of 85 kDa (CIN85) is a protein expressed in many different cell types, involved in processes as diverse as cytokinesis,[7] lysosomal degradation of the epidermal growth factor receptor,[8,9] clathrin-mediated receptor internalization,[10] cell adhesion and cytoskeletal remodeling,[11,12] and both T cell receptor[13] and B cell receptor (BCR) signaling.[14−18] In the context of processes associated with BCR signaling, CIN85 was shown to be constitutively associated with Src homology 2 domain-containing leukocyte protein of 65 kDa (SLP65),[15] engaging in promiscuous multivalent interactions between its Src-homology 3 (SH3) domains and SLP65 proline-rich motifs (PRMs).[18] By association with small unilamellar phospholipid vesicles via the N-terminal domain of SLP65, all these transient interactions lead to the formation of

Received: September 1, 2023
Revised: November 29, 2023
Accepted: November 30, 2023

https://doi.org/10.1021/jacs.3c09586
J. Am. Chem. Soc. XXXX, XXX, XXX−XXX

droplets showing characteristics of liquid−liquid phase separation (LLPS).[17,18] These organelles form in the resting state of the B cell and provide preformed complexes of CIN85 and SLP65, which allow for an accelerated cellular response upon BCR engagement.[17] Notably, CIN85 is involved in the preassembly of effectors in resting T cells as well, but this involves a distinctly different set of interaction partners compared to B cells.[13] Besides being necessary for the formation of droplets together with SLP65 in the resting state of the B cell, CIN85 itself also promotes higher-order structures: its C-terminal coiled-coil domain exhibits a high propensity for trimerization.[17] In addition to the heterotypic interactions, PRMs inside the protein can compete with other motifs for binding to the SH3 domains.[6,19] In summary, the multitude of possible interactions leads to a complex network of transient interactions characteristic of proteins serving different contextual functions. However, how the cellular context leads to differential behavior of multidomain proteins in distinct signaling pathways is still poorly understood. Dynamic regulation of these proteins is often facilitated by PTMs, such as phosphorylation at Tyr, Ser, or Thr residues.[20] Consequently, a common mode of regulation for multidomain proteins containing flexible linker regions is autoinhibition.[21] This is commonly caused by recognition motifs inside flexible linker or tail regions, occupying one of the domains completely until the interaction is perturbed. This results in the domain being able to engage with other effectors and/or become catalytically active.[22] There is evidence by previous studies that CIN85 SH3 domains are able to recognize PRMs within disordered regions of CIN85, leading to intra- or intermolecular autoinhibition.[6,19,23,24] Notably, Li et al. have provided indirect evidence of an autoinhibitory interaction mediated by the SH3C domain to the adjacent linker based on isothermal titration calorimetry experiments but did not investigate this further.[19] Because the propensity for LLPS is mainly driven by the interaction of CIN85 SH3 domains with SLP65 PRMs, this mechanism could be a powerful way for the intracellular modulation of LLPS. However, these interactions have not been characterized in detail in the context of multidomain protein constructs, leaving the extent of their overall contributions to CIN85 protein conformation and function an open question.

In this study, we identify a hitherto unknown PRM that predominantly interacts with the CIN85 SH3C domain. Using NMR spectroscopy, we characterize the interaction of the CIN85 SH3 domains with synthetic peptides, also addressing the influence of mutations on the binding. We assign the backbone resonances of the disordered linker containing the motif and investigate SH3:PRM binding via NMR relaxation and translational diffusion experiments in multidomain protein constructs of various lengths. We determined that this SH3:PRM interaction modulates the valency of the CIN85 protein and therefore the extent of interaction with its constitutive binding partner SLP65. Finally, we show the relevance of this interaction in DG75 B cell lymphoma cells for modulating B cell responses to stimulation of the BCR.

RESULTS

The Second IDR in CIN85 Contains a Novel PRM That Interacts Preferably with SH3C. We first investigated whether the linker regions in CIN85 were predicted to show deviations from a purely disordered linker. For this, we employed two predictors that are based on flexible regions in high-resolution X-ray structures (DISOPRED3[25]) and backbone flexibility from NMR chemical shifts of IDPs (DynaMine[26]). DISOPRED3 scores will be high for highly disordered sequences, while the DynaMine order parameter prediction indicates more rigid structures at high values. As displayed in Figure 1A, both predictors were able to distinguish

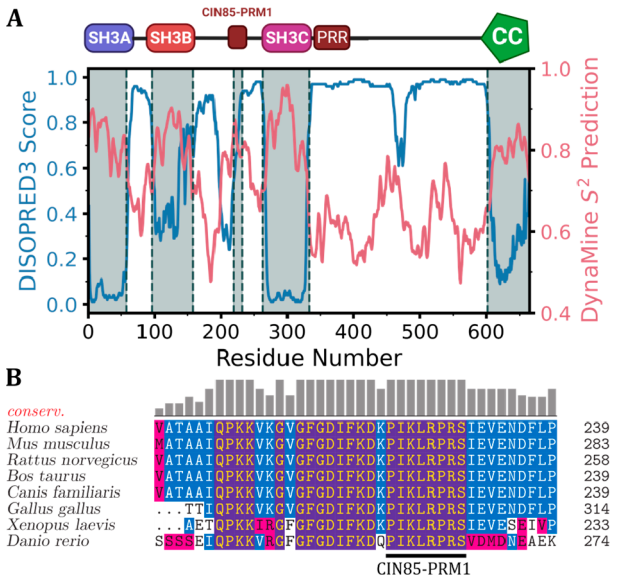

Figure 1. Sequence-based analysis of CIN85 linker regions. (A) Prediction of disorder (DISOPRED3[25]) and flexibility (DynaMine[26]) along the CIN85 amino acid sequence. DISOPRED3 scores will be close to one for highly disordered sequences, while the DynaMine order parameter prediction indicates more rigid structures at this value. (B) A multiple sequence alignment (MSA) of 7 representative CIN85 homologues shows the exceptional sequence identity between residues 200−239 of the human homologue. The MSA was generated with ClustalOmega[27] based on a BLAST[28] search of the CIN85 Uniprot entry Q96B97-1 (referenced to residues 200−239). The sequence conservation was plotted as bars at the top of each amino acid position.

the folded domains (SH3A-C and the coiled-coil (CC) domain) from the disordered linkers. In addition, both predictors show a significant deviation from a purely disordered sequence in the linker region between SH3B and SH3C (residues 162−263). Conserved residues in protein sequences can indicate functional importance, even in intrinsically disordered regions that typically do not show a high degree of conservation.[29] We therefore determined the sequence conservation within the intrinsically disordered linker between SH3B and SH3C by performing a BLAST[28] search starting from the CIN85 Uniprot entry Q96B97-1 and compared the sequence conservation between different CIN85 homologues (Figures 1B and Figure S1). Inside the region predicted by DynaMine to show the lowest flexibility, we identified a novel proline-rich sequence (residues 223−230) that showed exceptional sequence conservation among all homologues tested. It resembled the consensus sequence for PRM recognized by CIN85 SH3 domains (PXXXPR)[23] but contained an additional arginine residue (^{223}PIKL**R**PR^{229}). There is no known PRM in the CIN85 protein N-terminal to this motif, which is why we refer to it as "CIN85-PRM1" in the following.

We further used NMR titrations to assess the interaction of CIN85-PRM1 with isolated SH3 domains of CIN85, observing

https://doi.org/10.1021/jacs.3c09586
J. Am. Chem. Soc. XXXX, XXX, XXX−XXX

chemical shift perturbations (CSP) in the ^{15}N-labeled SH3 domains upon titration with a synthetic 14-residue peptide of the sequence ^{219}FKDKPIKLRPRSIE^{232} (see Figure S2). All three domains displayed moderate to weak affinity, with SH3C showing 3- and 5-fold lower dissociation constants (K_D) than SH3A and SH3B, respectively (K_D ~ 0.2−1.1 mM; see Table 1). This suggested the SH3C domain to be the dominant

Table 1. Dissociation Constants (K_D) of the Binary SH3:Peptide Interactions as Determined by NMR Titrations[a]

domain	peptide	K_D (mM)
SH3A	^{219}FKDKPIKLRPRSIE^{232}	0.73 ± 0.02
SH3B	^{219}FKDKPIKLRPRSIE^{232}	1.09 ± 0.05
SH3C	^{219}FKDKPIKLRPRSIE^{232}	0.21 ± 0.01
SH3C	^{219}FKDKPIKL**A**PRSIE^{232}	0.75 ± 0.01
SH3C	^{219}FKDKPIKLRP**A**SIE^{232}	2.45 ± 0.27
SH3C	^{219}FKDKPIKL**A**P**A**SIE^{232}	≫2.45
SH3C	^{219}FKDKPIKLRPR**pS**IE^{232}	2.35 ± 0.08
SH3C	^{219}FKDKPIKLRPR**A**IE^{232}	0.20 ± 0.01
SH3C	^{219}FKDKPIKLRPR**D**IE^{232}	0.71 ± 0.03

[a]The error in the fitted K_D values was determined via a bootstrap resampling approach.

interaction partner to CIN85-PRM1. We mapped the CSP onto the first model of the NMR structure of SH3C (PDB: 2k9g) in Figure 2A. Binding to the CIN85-PRM1 peptide occurs through the conserved binding site, involving the RT-loop (residues 278−292), the N-Src-loop (residues 300−307), and also the 3_{10}-helix (residues 320−322) of SH3C (see Figure 2B).

The recognition of PRM by SH3 domains typically depends on the presence of positively charged residues, such as arginines at the motif's N- or C-terminus, which often form cation−π interactions with conserved tryptophan residues in the SH3 binding interface.[30] In past studies on similar systems, the introduction of R/A mutations was found to be effective in perturbing this type of interaction.[15,17,23,31] We therefore used CIN85-PRM1 mutant peptide binding to the SH3C domain to determine the role of both arginines (R227 and R229) in this interaction. The K_D increased 4-fold for the R227A and 12-fold for the R229A mutant, with complete abolition of binding only after mutating both residues (see Figure 2B, Table 1, and Figure S3). The two arginine residues therefore contribute to the interaction to a different extent, with R229 playing a larger role. Because we knew that this interaction was in part driven by cation−π interactions, we anticipated a net energetic contribution on the order of −12 ± 6 kJ/mol if such an interaction would be disturbed by the mutation.[32] Indeed, we found this difference to be 3.28 ± 0.20 kJ/mol for the R227A mutant and 6.32 ± 1.00 kJ/mol for the R229A mutant peptides based on their K_D's. The difference in binding energy compared to wild-type peptide was consistent with the loss of a weak cation−π interaction for the R229A mutant, while for R227A, a specific interaction was unlikely, and this residue is more likely involved in nonspecific interactions within the binding interface. We suggest that both R227 and R229 tune the interaction in synergy, with R229 contributing most to the binding affinity, thus being potentially involved in a more persistent, specific interaction. Interpreting these results, one must bear in mind that these differences in binding energy

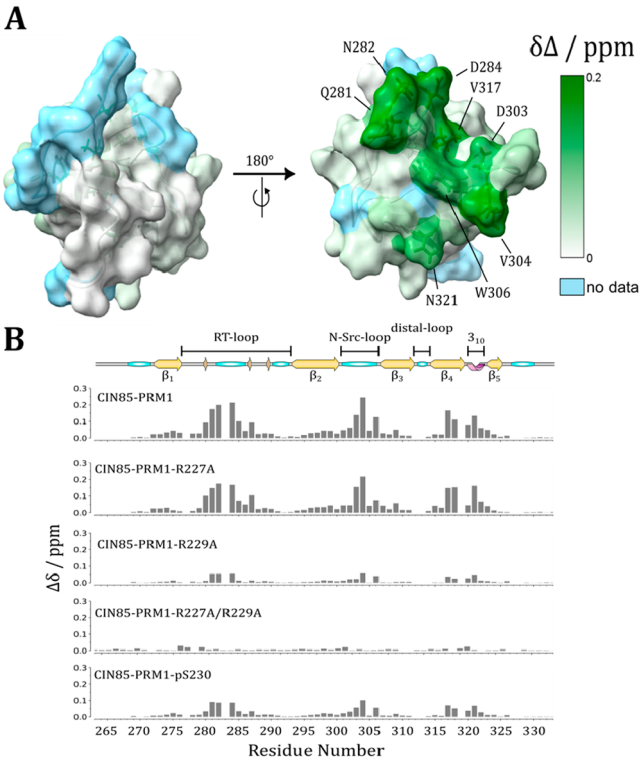

Figure 2. Interaction of CIN85 SH3C with CIN85-PRM1 peptides. (A) Chemical shift mapping of residues inside the SH3C domain exhibiting CSP (colored in shades of green) when titrated with an excess of the wild-type CIN85-PRM1 peptide. Residues for which no assignment was available are colored light blue. The SH3C domain structure used here was the first structure of the NMR ensemble deposited in the PDB as entry2k9g. (B) Bar plots showing the CSP of the residues within the SH3C domain in response to titration with the indicated CIN85-PRM1 peptides. For all the data shown, the molar ligand:protein ratio was chosen to be similar, ranging from 10.8 to 12.9. The secondary structure graph of SH3C on top of this figure was generated from the STRIDE[36] prediction of the PDB entry 2k9g using the SSS-Drawer Python script (https://github.com/zharmad/SSS-Drawer).

come from NMR titrations of a synthetic peptide with an isolated SH3 domain. In the context of the whole protein, local concentration and/or cooperative effects could increase the actual strength of this interaction considerably. The residue S230 is adjacent to R229 and a known site for activation-induced phosphorylation in CIN85[33,34] (see also Figure S4). To investigate the effect of S230s involvement in this interaction, we incorporated a phosphoserine (pS230), a S230D, and a S230A mutation into the synthetic peptide. We observed a similar increase in the K_D for pS230 as for the R229A mutation, while it was not at all affected by the S230A mutation (see Figure 2B and Table 1). This was consistent with a role of this residue in tuning the extent of interaction with CIN85-PRM1 only by post-translational modification while not being involved in the interaction in general. The phosphomimetic mutation S230D led to a much smaller increase in K_D, suggesting a specific role of the phosphoryl group in terms of electronegativity and excluded volume.[35] By correlating the CSP of mutated peptides and the wild-type peptide, we also determined that the mode of interaction was conserved, and differences in dissociation constants were only due to weakening of the interaction (Figure S5).

https://doi.org/10.1021/jacs.3c09586
J. Am. Chem. Soc. XXXX, XXX, XXX−XXX

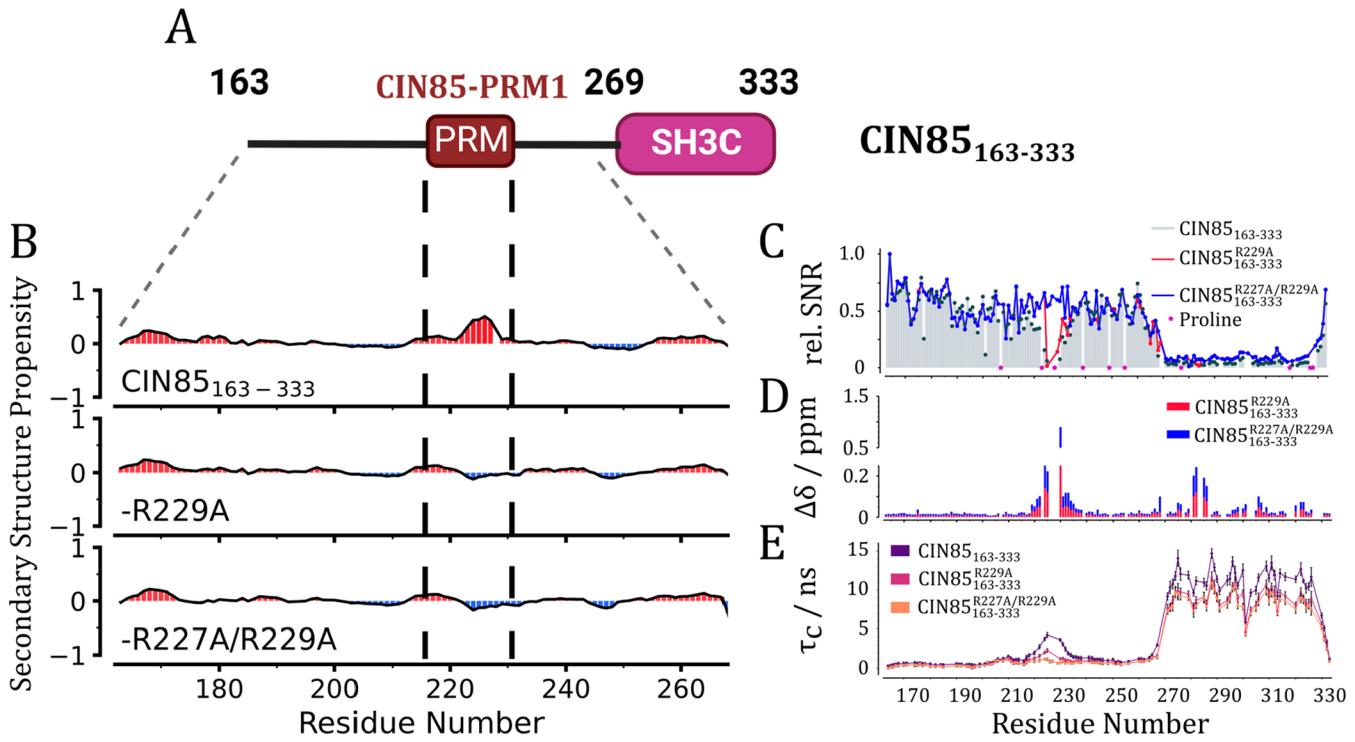

Figure 3. Determination of dynamical and structural properties of $CIN85_{163–333}$. (A) Domain architecture of $CIN85_{163–333}$. (B) Secondary structure propensities based on the backbone resonance assignment of $CIN85_{163–333}$ and the two arginine mutants $CIN85_{163–333}$-R229A and $CIN85_{163–333}$-R227A/R229A were calculated by using the ncSPC webserver.[37] Positive values in red indicate propensity for helical structures, while negative values report on propensity to form extended structures. (C) Relative signal/noise ratios of cross-peaks from the ^{13}C-detected HNCO spectra normalized to the C-terminal residue I164 for $CIN85_{163–333}$(gray bars), $CIN85_{163–333}$-R229A (red line), and $CIN85_{163–333}$-R227A/R229A (blue line). Proline residues were marked with magenta stars because they did not give rise to signals in the ^{13}C-detected HNCO spectra. (D) CSP of cross-peaks from the ^{13}C-detected HNCO spectra for $CIN85_{163–333}$-R229A (red) and $CIN85_{163–333}$-R227A/R229A (blue) compared to the $CIN85_{163–333}$ chemical shifts. (E) Residue-specific rotational correlation times for the three $CIN85_{163–333}$ constructs were determined using the TRACT experiment.[39] The protein samples were uniformly ^{13}C/^{15}N-labeled at a concentration of 1 mM. All experiments were acquired at 800 MHz and a temperature of 298 K.

CIN85-PRM1 Forms Helical Structures upon Interaction to SH3C. To study the potential interaction of the SH3C domain with CIN85-PRM1 in more detail, we needed to assign the linker backbone resonances first. We accomplished the near-complete assignment of the linker region containing CIN85-PRM1 by acquiring three-dimensional ^{13}C-detected experiments on a shorter construct of the CIN85 protein ($CIN85_{163–333}$; see Figure S6 for the different protein constructs used in this work and the spectral quality in Figure S7). Details of the resonance assignment process, including the assigned ^{13}C–^{15}N CON spectrum of $CIN85_{163–333}$, can be found in the Supporting Information. The backbone resonance assignments of $CIN85_{163–333}$, $CIN85_{163–333}$-R229A, and $CIN85_{163–333}$-R227A/R229A were deposited as BMRB entries 52081, 52080, and 52079, respectively. Within the disordered linker region (residues 163−263), we were successful in assigning 97% the backbone resonances, including the prolines inside CIN85-PRM1. Notably, some of the cross-peaks belonging to the core of CIN85-PRM1 were missing from the 3D spectra (L226N-K225C, R227N-L226C, and R229N-P228C). This was likely due to intermediate-exchange line broadening due to the interaction of SH3C with the PRM. This is illustrated here by the signal/noise ratio (SNR) of cross-peaks in the ^{13}C-detected HNCO spectra of $CIN85_{163–333}$ and of two arginine mutants showing reduced interaction to SH3C in the titration experiments (R229A and R227A/R229A; see Figure 3C). The resonances within CIN85-PRM1 were severely broadened in both $CIN85_{163–333}$ and the R229A mutant. Only upon introducing the R227A/R229A mutation did we observe the SNR increase to the level of the surrounding linker.

Significant CSPs were observed within CIN85-PRM1 (residues 280−285) and the RT-loop (residues 300−306) of the SH3C domain, consistent with the NMR titration results of CIN85-PRM1 peptides to the SH3C domain (see Figures 3D and 2B). Additionally, the secondary structure propensities (SSP) were predicted from the assigned chemical shifts using the ncSPC webserver[37] and showed a distinct propensity for helical structures within CIN85-PRM1 (Figure 3B). Torsion angles predicted using TALOS-N[38] were consistent with a 3_{10} helix formed by I224, K225, and L226. This was lost upon introduction of the R/A mutations (Figure 3B). We assigned the resonances of the free peptide in order to determine whether the helical structures within CIN85-PRM1 form upon binding or are already present in the free peptide but disrupted by the R/A mutations (Figures S8 and S9). We found no significant propensity for helix in the free peptide and the helical structure thus likely forms through a disorder-to-order transition upon binding to SH3C. This is consistent with known structures of SH3 domains bound to their respective peptides,[40−42] e.g., the complex between GADS-SH3C and a SLP76-peptide (Figure S10A). For that complex, it was shown that the 3_{10} helix within the peptide forms similarly through a disorder-to-order transition.[41]

https://doi.org/10.1021/jacs.3c09586
J. Am. Chem. Soc. XXXX, XXX, XXX−XXX

Small Bound-State Population of CIN85$_{163-333}$ Based on Local Correlation Times. We further used the TRACT[39] experiment to determine residue-specific apparent rotational correlation times (τ_c) within CIN85$_{163-333}$ and sample the interaction between SH3C and CIN85-PRM1 (Figure 3E). We observed small local correlation times τ_c for linker residues outside of CIN85-PRM1 and an increase within its core for CIN85$_{163-333}$ (τ_c = 4.3 ns). The R229A mutant showed a distinct decrease in τ_c of residues within CIN85-PRM1 (τ_c = 2.3 ns), and for the R227A/R229A mutant there was no significant difference to the surrounding linker (τ_c = 0.5−1 ns). Here, we focused on the residues within CIN85-PRM1 with the highest correlation time, as these determine the bound fraction. The smaller correlation times of other residues within the motif can be explained by the individual binding behaviors of the amino acids and the variability in complexes formed through fuzzy interactions. Clearly, even in wild-type CIN85$_{163-333}$ none of the residues of CIN85-PRM1 showed the τ_c of the SH3C domain, averaging at around 11 ns. Bound fractions were estimated based on maximum local correlation times in CIN85-PRM1 and the average correlation time of the SH3C domain. This was calculated to be 31% for CIN85$_{163-333}$, 14% for the R229A mutant, and zero for the R227A/R229A mutant. For an isolated SH3 domain at room temperature, global τ_c values are generally found between 4 and 5 ns.[43] The elevated τ_c for the SH3C domain can be explained mainly by the presence of the linker, as control experiments with the isolated SH3C domain showed distinctly lower apparent τ_c in its absence (Figure S11). Disordered tails are known to cause a significant amount of drag on the folded domain, slowing down its reorientational dynamics.[44,45] The interaction between CIN85-PRM1 and the SH3 domain led to another small increase in the apparent τ_c within the SH3C domain compared to the R227A/R229A mutant where binding is abolished (see Figure 3E).

Arginine Side-Chain Rotational Dynamics Indicate Competition between Both Arginines in CIN85-PRM1. Because the arginine residues were arguably playing a major role in this interaction, we further probed rotational dynamics of the arginine guanidinium groups in CIN85$_{163-333}$ through multiquantum chemical exchange saturation transfer (MQ-CEST)[46] experiments. These allow us to sample the restricted rotation of the guanidinium group mediated by noncovalent interactions such as salt bridges and cation−π interactions (Figures S12−S14). Unlike R176, R227, and R265 in the disordered linker and R314 and R315 in the SH3C domain, no N^{ε}−H^{ε} cross-peak was observed for the side chain of R229, consistent with its involvement in a salt bridge or cation−π interaction resulting in signal broadening (Figure S12). The rate of rotation (k_{ex}) around the C^{ζ}−N^{ε} bond of the free arginine guanidinium group was 397 ± 4 s^{-1}, in close agreement with previous reports.[46,47] The obtained k_{ex} rates for R176 and R227 were smaller than free arginine but larger than those of R314 and R265/R315 (Figure S14A), indicating the less restricted rotational dynamics of arginine side chains in the disordered linker region than in the folded domain. Upon removal of R229 in the CIN85$_{163-333}$-R229A mutant, a small but significant reduction in k_{ex} was observed for R227, while no significant change in k_{ex} was detected for the other arginines. The chemical shift separation $\Delta\omega$ between the two N^{η} nuclei exhibited a similar trend, increasing significantly only for R227 in the R229A mutant compared to wild-type CIN85$_{163-333}$ (Figure S14B). This intriguing observation may suggest a degree of competition between R227 and R229 in the interaction with SH3C, so that the partial interaction of R227 with SH3C becomes possible only when R229 is absent. The comparatively small effect of the R229A mutation on R227 arginine side-chain rotational dynamics can be reconciled by the low bound fractions for both constructs determined via the TRACT experiments. As k_{ex} is a population-averaged value, we would expect the difference to increase with the population of the bound state. In short, the MQ-CEST data provided additional support for the involvement of residue R229 in the CIN85-PRM1:SH3C interaction in the wild-type protein and suggested a role for residue R227 in this interaction after the R229A mutation.

Effective Concentration Effects Favor the Interaction of SH3C to CIN85-PRM1. For recognition motifs tethered to their receptor, effective concentration (c_{eff}) effects have been shown to have a significant influence on binding.[48,49] To understand the role of c_{eff} in the SH3C:CIN85-PRM1 interaction, we estimated c_{eff} of SH3C at CIN85-PRM1 using protein:peptide-complex structures predicted by HADDOCK.[50,51] We used residues with significant CSP in peptide titration experiments to guide the docking process and measured the distance between the last residue of the folded domain and the beginning of the binding motif to obtain the relevant distance in the complex structure based on the approach developed by Kjærgaard et al.[52] The effective concentration of the predicted complexes was found to be in the range 1.3−6.3 mM, while the K_D obtained from titration of the untethered CIN85-PRM1 peptide to SH3C was 0.2 mM, indicating well-saturated binding in all complexes (Figures S15 and S16). The population of the bound, i.e., autoinhibited, state calculated from these effective concentrations was between 0.86 and 0.97. Because the three SH3 domains are highly related, we further assumed that the same relevant distances as for SH3C should be applicable to the potential intramolecular complexes between these domains and CIN85-PRM1. We found c_{eff} to range between 0.9 and 1.3 mM for the SH3A domain and 1.6−4.1 mM for the SH3B domain. This translated to a factor of 30 (SH3C) > 4 (SH3B) > 2 (SH3A) in comparison with the dissociation constants to the free peptide (Table 1). Therefore, the interaction of SH3C with CIN85-PRM1 is likely to be favored over both remaining SH3 domains based on c_{eff} and K_D. The small bound fraction determined for the wild-type construct (about 31%) was inconsistent with the expected results from the c_{eff} calculations in this paragraph. However, it is known that disordered regions can behave differently depending on whether they are tethered to folded domains on one or both ends.[53] A disordered tail, as in CIN85$_{163-333}$, is likely to behave as an "entropic bristle", sampling a large conformational space and therefore making a specific interaction with SH3C less likely.[54−56]

The SH3C Domain in CIN85$_{1-333}$ Is Autoinhibited by Binding to CIN85-PRM1 Intramolecularly. In contrast to a disordered tail, a linker tethered on both ends will likely have a decreased entropic chain character. This can have the opposite effect compared to the disordered tail, maximizing the local domain concentration and thereby enforcing an intramolecular interaction.[57] To test whether the population of the bound state was indeed larger in the longer CIN85$_{1-333}$, we transferred the assignment of the linker region from the truncated CIN85$_{163-333}$ by comparing their ^{1}H−^{15}N TROSY spectra (Figures S17 and S18) and determined the apparent τ_c values for CIN85$_{1-333}$ and its R/A mutants (Figure 4B). The

https://doi.org/10.1021/jacs.3c09586
J. Am. Chem. Soc. XXXX, XXX, XXX−XXX

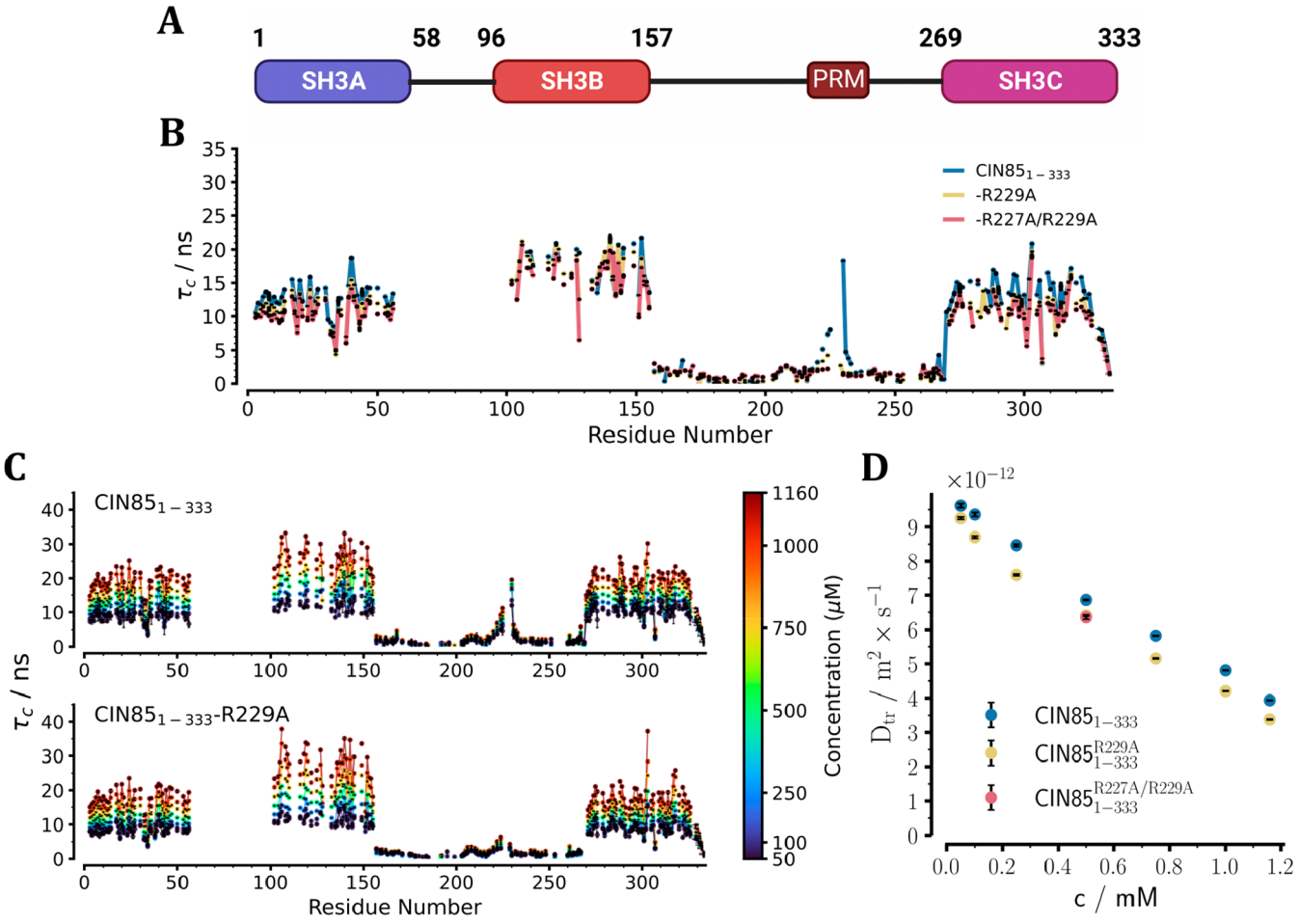

Figure 4. Determination of intermolecular nonspecific transient interactions as well as intramolecular specific interactions in $CIN85_{1-333}$. (A) Domain architecture of $CIN85_{1-333}$. (B) Residue-specific rotational correlation time of the three $CIN85_{1-333}$ constructs at a molar concentration of 0.5 mM using the TRACT experiment.[39] (C) Residue-specific apparent rotational correlation times of $CIN85_{1-333}$ and $CIN85_{1-333}$-R229A in dependence of protein concentration ranging from 0.05 to 1.16 mM. (D) Translational diffusion coefficient D_{tr} of $CIN85_{1-333}$ (blue) and $CIN85_{1-333}$-R229A (yellow) determined using the N-TRO-STE experiment[58] in dependence of protein concentration ranging from 0.05 to 1.16 mM. The R227A/R229A mutant of $CIN85_{1-333}$ (red) was sampled at a single concentration (0.5 mM). The $CIN85_{1-333}$ constructs used here were expressed uniformly as ^{15}N-labeled and perdeuterated. All experiments were conducted at 800 MHz and 298 K.

residue S230 was used here as a proxy for the apparent τ_c of the CIN85-PRM1 core because residues L226-R229 could not be assigned in the $^1H-^{15}N$ TROSY spectrum of $CIN85_{1-333}$. Indeed, we observed a significantly higher population of the bound state in $CIN85_{1-333}$, characterized by a distinct increase in τ_c of residue S230 (τ_c^{S230} = 18.3 ns at 0.5 mM). As for the shorter $CIN85_{163-333}$, the R229A and R227A and R229A mutations were effective in abolishing this interaction. In comparison, the median τ_c for the three SH3 domains at this concentration ranged between 12.7 and 18.2 ns (Figure S19). Some residues such as D303 (part of the n-Src loop of SH3C; see also Figure 2B) exhibited values significantly larger than these median values (τ_c^{D303} = 20.9 ns at 0.5 mM). The elevated τ_c observed for S230 can, therefore, be explained by the interaction of CIN85-PRM1 with the binding interface of one of the SH3 domains.

To determine whether the interaction with CIN85-PRM1 was dominated by an intramolecular or intermolecular binding mode, we further analyzed residue-specific τ_c values and translational diffusion coefficients D_{tr} over a wide concentration range for $CIN85_{1-333}$ and its R229A mutant (Figure 4C,D). The R229A mutant was chosen as a control because it already sufficiently perturbed the interaction with CIN85-PRM1 (Figure 4B). In $CIN85_{1-333}$, we found the ratio of τ_c values between residues within CIN85-PRM1 and the SH3 domains to be independent of concentration, proving that the interaction was intramolecular. As expected, the R229A mutant showed small τ_c values within CIN85-PRM1 at all concentrations, more similar to those of the surrounding linker. These findings were corroborated by the translational diffusion coefficients (D_{tr}) determined via N-TRO-STE experiments[58] (Figure 4D). $CIN85_{1-333}$ consistently showed higher D_{tr} values than the R229A mutant did at all concentrations, indicating slower translational motion of the mutant (6%−14% difference, depending on concentration) and consequently a more compact shape of $CIN85_{1-333}$ compared to $CIN85_{1-333}$-R229A. In addition to the differences between constructs indicating the intramolecular SH3-PRM association, we also observed effects common to both $CIN85_{1-333}$ and the R229A mutant. These showed a general concentration dependence of local apparent τ_c within the SH3 domains and the global D_{tr} (Figure 4C,D). We also found the slope of the concentration dependence of D_{tr} for both constructs to be the same within the experimental uncertainty (Figure S20). This showed the

https://doi.org/10.1021/jacs.3c09586
J. Am. Chem. Soc. XXXX, XXX, XXX−XXX

concentration dependence of these parameters to be independent of the interaction with CIN85-PRM1 and thus common to both constructs. To rule out the possibility that viscosity changes with protein concentration were mainly responsible for the observed differences, we measured ^{17}O T_1 relaxation rates of bulk water in the buffer at different protein concentrations and estimated the resulting viscosity changes[59] (Figure S21). The measured dynamic viscosity increased by a factor of 1.32 from pure buffer to a $CIN85_{1-333}$ concentration of 1.3 mM. However, the median rotational correlation time of the three SH3 domains in $CIN85_{1-333}$ and the R229A mutant increased by a factor of 1.9−2.3 and 2.0−2.6, respectively (Figure S19). Consistently, we found this change to be a factor of 2.4 and 2.7 for D_{tr} (Figure 4D). Therefore, the observed differences in τ_c and D_{tr} with the concentration cannot be attributed to viscosity changes alone. These differences can be explained by assuming an increasing extent of transient nonspecific protein−protein interactions with concentration,[60,61] which however do not involve the CIN85-PRM1:SH3 interaction. Thus, in addition to the specific trimerization via the coiled-coil domain that has been described previously,[17] CIN85 SH3 domains can also mediate nonspecific low-affinity oligomerization by themselves.

CIN85-PRM1 Phosphorylated at S230 Provides an Activation-Induced Release of CIN85 SH3 Domains. The serine residue at position 230 was shown to significantly weaken the CIN85-PRM1:SH3 association in its phosphorylated state (Figure 2B and Table 1). In addition, it was found to be highly phosphorylated in a multitude of phosphoproteomic studies (Figure S4). In particular, S230 has been shown to be phosphorylated during tonic signaling in B cells[62] and in response to BCR engagement,[33] which is why we decided to assess the signaling function of this residue. We introduced fluorescently labeled full-length citrine (cit)-CIN85 and cit-CIN85-S230A into DG75 B cells expressing no endogenous CIN85. The intact BCR-related signaling machinery made this cell line suitable for studying the effect of the mutation on B cell signaling.[33] The S230A mutation was selected because it did not affect SH3C's interaction with the corresponding mutant peptide (see Table 1), and it created a mutant that could not be phosphorylated at position S230. It has been shown previously that the multivalent and promiscuous interactions between CIN85 SH3 domains and SLP65 PRMs drive the formation of liquid-like condensates that are a necessary prerequisite for BCR signaling events to occur.[18] Monitoring the propensity for LLPS is therefore a viable readout for the overall BCR-related signaling capabilities of the S230A mutant. Utilizing imaging flow cytometry, we observed a decrease in the percentage of droplet-positive cells and attenuated BCR-induced recruitment to the plasma membrane of the S230A variant compared to wild-type CIN85 (see Figure 5A,B). These findings correlated with compromised BCR-induced Ca^{2+} mobilization in CIN85-S230A-expressing DG75 B cells compared to cells producing the wild-type protein (Figure 5C). Hence, this indicated that the modulation of LLPS propensity by phosphorylation at S230 is a probable scenario for efficient BCR-induced signaling via liquid-like condensates, corroborating what has been shown previously by Wong et al.[18]

We further used label-free mass spectrometry to investigate how phosphorylation of CIN85-PRM1 changes the CIN85 interactome. For this purpose, we purified CIN85 from lysates of DG75 B cells expressing either wild-type cit-CIN85 or cit-CIN85-S230A, in both the resting and stimulated state (see Figures S22 and S23). Comparing the abundance of proteins interacting with cit-CIN85 relative to cit-CIN85-S230A, this approach did not reveal any specific protein interacting with CIN85-PRM1 in either the resting or stimulated state. Therefore, we could exclude that a specific interaction was lost upon introducing the S230A mutation. This also indicated that phosphorylated S230 had no specific interaction partner, and its sole function in the context of BCR signaling might be the modulation of the interaction between CIN85-PRM1 and SH3C. Nevertheless, we observed more subtle differences in the interactome of CIN85. We determined decreased abundances of both SLP65 and CIN85 in preparations of the S230A variant. Because we did not detect a difference in

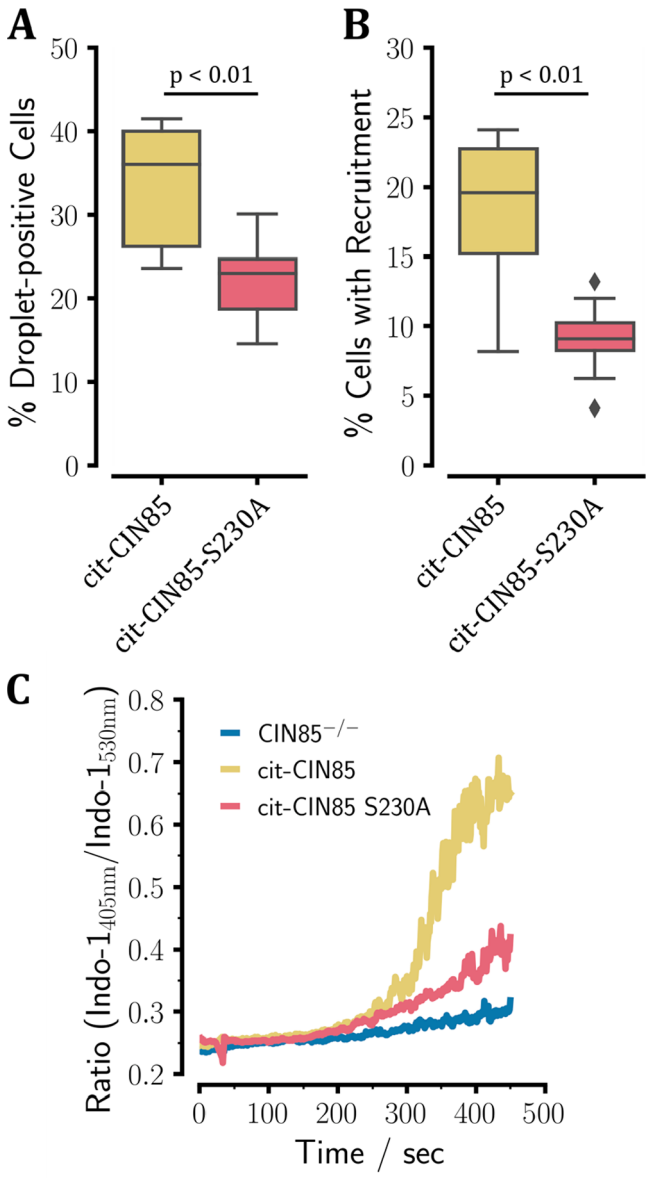

Figure 5. : Imaging flow-cytometric characterization of DG75 B cells carrying cit-CIN85 (yellow) or cit-CIN85-S230A (red). (A) Percentage of DG75 B cells that showed cytosolic droplets. (B) Percentage of DG75 B cells that exhibited significant recruitment of CIN85 to the plasma membrane. (C) Ca^{2+}-mobilization sampled as the ratio of the Indo-1 absorbance ratio 405 nm/530 nm using DG75 B cells carrying either cit-CIN85 (yellow), cit-CIN85-S230A (red), or $CIN85^{-/-}$ knockouts (blue).

https://doi.org/10.1021/jacs.3c09586
J. Am. Chem. Soc. XXXX, XXX, XXX−XXX

the expression of the mutant compared to the wild type (Figure S24), this can likely be attributed to the reduced propensity for these two proteins to engage in network formation leading to liquid-like condensates (Figure 5A).

DISCUSSION

The interaction networks mediated by scaffold proteins such as CIN85 and SLP65 have been shown to be of primary importance for the physiological signaling processes occurring in human and murine B cells.[63,64] Previous work addressed the assembly of these two scaffolds into liquid-like presignaling clusters that are a prerequisite for the proper function of BCR signaling and enable a rapid cellular response upon BCR engagement.[15−18] Yet, open questions still exist regarding the necessary modifications in CIN85 and SLP65 to modulate their propensity for undergoing LLPS and to enable a signaling-competent state. The CIN85 protein serves a multitude of different context-sensitive functions in a variety of different cell types, which require finely balanced and tightly controlled regulation. In multidomain proteins, an effective way of providing regulation by the cell is through a SH3-mediated intramolecular association involving IDRs. This recurring theme of autoinhibited SH3 domains has been observed for several different systems in immune cells, including the Nck adaptor protein in T cells[65] and the cytosolic component of the NADPH oxidase $p47^{phox}$ in phagocytes.[66] From the perspective of cellular signaling, regulation by intramolecular interactions has the advantage of being concentration independent and, due to effective concentration effects, needing only moderate nominal affinities to compete with potential intermolecular binding partners.

Based on our findings, we therefore suggest that one of the SH3 domains is autoinhibited by the intramolecular interaction with CIN85-PRM1 in the adjacent linker region. From the nature of the NMR relaxation experiments presented here (Figure 4B,C), we can only definitively say that the bound state is the major populated state, but not whether one or multiple of the domains enforce this interaction synergistically. However, we observed a clear hierarchy of binding affinities of the different SH3 domains to CIN85-PRM1, with SH3C binding the strongest, followed by SH3A and SH3B (Table 1). This hierarchy is also supported by the phylogenetic origin of these domains, as SH3B and SH3C have split from the common progenitor SH3 domain first, while the SH3A domain was later generated via gene duplication of SH3C, making them more similar compared to SH3B.[67] This also reflects the fact that SH3A and SH3B exhibit strikingly dissimilar binding mechanisms to similar peptides.[68] In addition, our analysis of dissociation constants and effective concentrations suggests that SH3C is likely to outcompete SH3A and SH3B (Table 1, Figures S15 and S16). Therefore, based on the data at hand, we argue that CIN85-PRM1 is able to compete with SLP65 PRM's for binding to SH3C and is fully bound by the domain while the SH3A and SH3B domains are free to engage with SLP65.

The given state of a multidomain scaffold protein like CIN85 is typically determined by the presence or absence of many different nominally low-affinity interactions. The autoinhibitory interaction between the SH3C domain and CIN85-PRM1 is thus a potential candidate for shifting these equilibria toward a signaling-competent state of the CIN85 protein upon engagement of the BCR. Having established the autoinhibition of the SH3C domain *in vitro*, we addressed its potential signaling consequences in the cellular context. Because the promiscuous interactions of CIN85 SH3 domains with SLP65 PRMs drive the LLPS in conjunction with small vesicles,[18] modulating the valency of the CIN85 protein should also have an effect on the propensity for phase separation. Indeed, a study conducted in parallel by our group has investigated the phase separation behavior of CIN85 and SLP65 by *in vitro* droplet reconstitution assays and lattice-based computational modeling.[31] One main finding of that study was that the threshold concentration for LLPS was lowered for the $CIN85_{1-333}$-R227A/R229A mutant in which the interaction between SH3C and CIN85-PRM1 was abolished (see Figure S8 in Maier et al.[31]). This can be understood quantitatively only if one assumes the presence of an autoinhibitory interaction, preventing one of the SH3 domains from interacting with SLP65 PRMs. These results are therefore consistent with the proposed autoinhibition of the SH3C domain, as discussed above. The activation-induced phosphorylation of S230, located directly adjacent to CIN85-PRM1 (Figure 1B), has been shown to occur shortly after the stimulation of the BCR.[33] Taking into account the presented evidence of the intramolecular interaction between SH3C and CIN85-PRM1 *in vitro*, we suggest that this motif acts as a "switch" to modulate CIN85's valency depending on the cellular signaling state. The data from cultured B cells presented here support this hypothesis, as the propensity for LLPS was significantly decreased in the cit-CIN85-S230A mutant cells, where this interaction is expected to be persistently active (Figure 5A). This also suggests a significant population of phosphorylated CIN85-PRM1 in the state of tonic signaling[62,69] because this difference was already apparent in the nonstimulated cells. Modulating the extent of this interaction could therefore help to maintain the correct level of LLPS in resting B cells and shift the equilibrium depending on their cellular activation state. This in turn can influence the response of these cells to external stimuli, which was evident here from the reduced recruitment of CIN85 to the plasma membrane and the diminished mobilization of Ca^{2+} in response to BCR engagement (see Figure 5B,C).

In conclusion, we propose a mechanism by which the SH3C domain of CIN85 is autoinhibited by an intramolecular interaction to CIN85-PRM1. This interaction is regulated intracellularly through phosphorylation at neighboring residue S230, which upon phosphorylation enables the SH3C domain to engage in interactions with SLP65 and other effectors, promoting the physiological signaling-competent state. We further propose that the modulation of the interaction between CIN85 SH3 domains and CIN85-PRM1 is important for maintaining the preformed signaling clusters of CIN85 and SLP65 to allow for a dynamic and contextual response depending on the cellular activation state.

ASSOCIATED CONTENT

Supporting Information

The Supporting Information is available free of charge at https://pubs.acs.org/doi/10.1021/jacs.3c09586.

Experimental section; resonance assignment of flexible linker regions in CIN85 using a combination of ^{1}H- and ^{13}C-detected NMR experiments; determination of intramolecular effective concentrations from HADDOCK-derived complex structures; determination of arginine

https://doi.org/10.1021/jacs.3c09586
J. Am. Chem. Soc. XXXX, XXX, XXX−XXX

side-chain dynamics using MQ-CEST experiments (PDF)

Mass spectrometric analysis of protein abundances in DG75 B cells (XLSX)

AUTHOR INFORMATION

Corresponding Author

Christian Griesinger − *Department for NMR-based Structural Biology, Max Planck Institute for Multidisciplinary Sciences, 37077 Göttingen, Germany;* orcid.org/0000-0002-1266-4344; Email: cigr@mpinat.mpg.de

Authors

Daniel Sieme − *Department for NMR-based Structural Biology, Max Planck Institute for Multidisciplinary Sciences, 37077 Göttingen, Germany;* orcid.org/0000-0001-9000-9938

Michael Engelke − *Institute for Cellular and Molecular Immunology, Georg-August University Göttingen, 37073 Göttingen, Germany*

Nasrollah Rezaei-Ghaleh − *Institute of Physical Biology, Heinrich Heine University Düsseldorf, 40225 Düsseldorf, Germany; Institute of Biological Information Processing, IBI-7: Structural Biochemistry, Forschungszentrum Jülich, 52428 Jülich, Germany;* orcid.org/0000-0001-6935-6564

Stefan Becker − *Department for NMR-based Structural Biology, Max Planck Institute for Multidisciplinary Sciences, 37077 Göttingen, Germany*

Jürgen Wienands − *Institute for Cellular and Molecular Immunology, Georg-August University Göttingen, 37073 Göttingen, Germany*

Complete contact information is available at: https://pubs.acs.org/10.1021/jacs.3c09586

Funding

This work was supported by the Max Planck Society. We thank the DFG (Deutsche Forschungsgemeinschaft) for support in the framework of the SFB860 project B05. N.R.-G. acknowledges the DFG for research grant RE 3655/2-3. Open access funded by Max Planck Society.

Notes

The authors declare no competing financial interest.

ACKNOWLEDGMENTS

The authors thank Claudia Schwiegk for the expression and purification of the recombinant protein samples used throughout this work and Kerstin Overkamp for the synthesis of the peptides used in the titration experiments. We are grateful to Gogulan Karunanithy and D. Flemming Hansen for providing the MQ-CEST pulse programs and analysis scripts and to Joachim Maier for useful discussions.

ABBREVIATIONS

BCR, B cell receptor; cit, citrine; CC, coiled-coil; CIN85, Cbl-interacting protein of 85 kDa; CSP, chemical shift perturbations; IDP, intrinsically disordered protein; IDR, intrinsically disordered region; LLPS, liquid−liquid phase separation; MQ-CEST, multiquantum chemical exchange saturation transfer; MSA, multiple sequence alignment; NMR, nuclear magnetic resonance; PRM, proline-rich motif; PTM, post-translational modification; SH3, Src-homology 3; SLP65, Src homology 2 domain-containing leukocyte protein of 65 kDa; SSP, secondary structure propensities; TRACT, TROSY for rotational correlation times; TROSY, transverse relaxation-optimized spectroscopy.

REFERENCES

(1) Good, M. C.; Zalatan, J. G.; Lim, W. A. Scaffold Proteins: Hubs for Controlling the Flow of Cellular Information. *Science* **2011**, *332* (6030), 680−686.

(2) Wong, W.; Scott, J. D. AKAP signalling complexes: focal points in space and time. *Nat. Rev. Mol. Cell Biol.* **2004**, *5* (12), 959−970.

(3) Levchenko, A.; Bruck, J.; Sternberg, P. W. Scaffold proteins may biphasically affect the levels of mitogen-activated protein kinase signaling and reduce its threshold properties. *Proc. Natl. Acad. Sci. U. S. A.* **2000**, *97* (11), 5818−5823.

(4) Ferrell, J. E. What Do Scaffold Proteins Really Do? *Sci. STKE* **2000**, *2000* (52), pe1−pe1.

(5) Burack, W. R.; Shaw, A. S. Signal transduction: hanging on a scaffold. *Curr. Opin. Cell Biol.* **2000**, *12* (2), 211−216.

(6) Havrylov, S.; Redowicz, M. J.; Buchman, V. L. Emerging roles of Ruk/CIN85 in vesicle-mediated transport, adhesion, migration and malignancy. *Traffic* **2010**, *11* (6), 721−731.

(7) Panagiotou, T. C.; Chen, A.; Wilde, A. An anillin-CIN85-SEPT9 complex promotes intercellular bridge maturation required for successful cytokinesis. *Cell Rep.* **2022**, *40* (9), 111274.

(8) Soubeyran, P.; Kowanetz, K.; Szymkiewicz, I.; Langdon, W. Y.; Dikic, I. Cbl-CIN85-endophilin complex mediates ligand-induced downregulation of EGF receptors. *Nature* **2002**, *416* (6877), 183−187.

(9) Haglund, K.; Shimokawa, N.; Szymkiewicz, I.; Dikic, I. Cbl-directed monoubiquitination of CIN85 is involved in regulation of ligand-induced degradation of EGF receptors. *Proc. Natl. Acad. Sci. U. S. A.* **2002**, *99* (19), 12191−12196.

(10) Kowanetz, K.; Terzic, J.; Dikic, I. Dab2 links CIN85 with clathrin-mediated receptor internalization. *FEBS letters* **2003**, *554* (1−2), 81−87.

(11) Schmidt, M. H. H.; Chen, B.; Randazzo, L. M.; Bögler, O. SETA/CIN85/Ruk and its binding partner AIP1 associate with diverse cytoskeletal elements, including FAKs, and modulate cell adhesion. *J. Cell Sci.* **2003**, *116* (14), 2845−2855.

(12) Hutchings, N. J.; Clarkson, N.; Chalkley, R.; Barclay, A. N.; Brown, M. H. Linking the T Cell Surface Protein CD2 to the Actin-capping Protein CAPZ via CMS and CIN85. *J. Biol. Chem.* **2003**, *278* (25), 22396−22403.

(13) Luff, D. H.; Wojdyla, K.; Oxley, D.; Chessa, T.; Hudson, K.; Hawkins, P. T.; Stephens, L. R.; Barry, S. T.; Okkenhaug, K. PI3Kδ Forms Distinct Multiprotein Complexes at the TCR Signalosome in Naïve and Differentiated CD4+ T Cells. *Front. Immunol.* **2021**, *12*, 631271.

(14) Watanabe, S.; Take, H.; Takeda, K.; Yu, Z.-X.; Iwata, N.; Kajigaya, S. Characterization of the CIN85 Adaptor Protein and Identification of Components Involved in CIN85 Complexes. *Biochem. Biophys. Res. Commun.* **2000**, *278* (1), 167−174.

(15) Oellerich, T.; Bremes, V.; Neumann, K.; Bohnenberger, H.; Dittmann, K.; Hsiao, H.-H.; Engelke, M.; Schnyder, T.; Batista, F. D.; Urlaub, H.; Wienands, J. The B-cell antigen receptor signals through a preformed transducer module of SLP65 and CIN85. *EMBO J.* **2011**, *30* (17), 3620−3634.

(16) Engelke, M.; Pirkuliyeva, S.; Kuhn, J.; Wong, L.; Boyken, J.; Herrmann, N.; Becker, S.; Griesinger, C.; Wienands, J. Macromolecular assembly of the adaptor SLP-65 at intracellular vesicles in resting B cells. *Sci. Signal.* **2014**, *7* (339), ra79−ra79.

(17) Kühn, J.; Wong, L. E.; Pirkuliyeva, S.; Schulz, K.; Schwiegk, C.; Fünfgeld, K. G.; Keppler, S.; Batista, F. D.; Urlaub, H.; Habeck, M.; Becker, S.; Griesinger, C.; Wienands, J. The adaptor protein CIN85 assembles intracellular signaling clusters for B cell activation. *Sci. Signal.* **2016**, *9* (434), ra66−ra66.

(18) Wong, L. E.; Bhatt, A.; Erdmann, P. S.; Hou, Z.; Maier, J.; Pirkuliyeva, S.; Engelke, M.; Becker, S.; Plitzko, J.; Wienands, J.;

Griesinger, C. Tripartite phase separation of two signal effectors with vesicles priming B cell responsiveness. *Nat. Commun.* **2020**, *11* (1), 848.
(19) Li, Q.; Yang, W.; Wang, Y.; Liu, W. Biochemical and Structural Studies of the Interaction between ARAP1 and CIN85. *Biochemistry* **2018**, *57* (14), 2132−2139.
(20) Gelens, L.; Saurin, A. T. Exploring the Function of Dynamic Phosphorylation-Dephosphorylation Cycles. *Dev. Cell* **2018**, *44* (6), 659−663.
(21) Trudeau, T.; Nassar, R.; Cumberworth, A.; Wong, E. T.; Woollard, G.; Gsponer, J. Structure and intrinsic disorder in protein autoinhibition. *Structure* **2013**, *21* (3), 332−341.
(22) Kliche, J.; Ivarsson, Y. Orchestrating serine/threonine phosphorylation and elucidating downstream effects by short linear motifs. *Biochem. J.* **2022**, *479* (1), 1−22.
(23) Kowanetz, K.; Szymkiewicz, I.; Haglund, K.; Kowanetz, M.; Husnjak, K.; Taylor, J. D.; Soubeyran, P.; Engstrom, U.; Ladbury, J. E.; Dikic, I. Identification of a novel proline-arginine motif involved in CIN85-dependent clustering of Cbl and down-regulation of epidermal growth factor receptors. *J. Biol. Chem.* **2003**, *278* (41), 39735−39746.
(24) Borthwick, E. B.; Korobko, I. V.; Luke, C.; Drel, V. R.; Fedyshyn, Y. Y.; Ninkina, N.; Drobot, L. B.; Buchman, V. L. Multiple Domains of Ruk/CIN85/SETA/CD2BP3 are Involved in Interaction with p85α Regulatory Subunit of PI 3-kinase. *J. Mol. Biol.* **2004**, *343* (4), 1135−1146.
(25) Jones, D. T.; Cozzetto, D. DISOPRED3: precise disordered region predictions with annotated protein-binding activity. *Bioinformatics* **2015**, *31* (6), 857−863.
(26) Cilia, E.; Pancsa, R.; Tompa, P.; Lenaerts, T.; Vranken, W. F. The DynaMine webserver: predicting protein dynamics from sequence. *Nucleic Acids Res.* **2014**, *42* (W1), W264−W270.
(27) Sievers, F.; Wilm, A.; Dineen, D.; Gibson, T. J.; Karplus, K.; Li, W.; Lopez, R.; McWilliam, H.; Remmert, M.; Söding, J.; Thompson, J. D.; Higgins, D. G. Fast, scalable generation of high-quality protein multiple sequence alignments using Clustal Omega. *Mol. Syst. Biol.* **2011**, *7* (1), 539.
(28) Altschul, S. F.; Gish, W.; Miller, W.; Myers, E. W.; Lipman, D. J. Basic local alignment search tool. *J. Mol. Biol.* **1990**, *215* (3), 403−410.
(29) Ota, H.; Fukuchi, S. Sequence conservation of protein binding segments in intrinsically disordered regions. *Biochem. Biophys. Res. Commun.* **2017**, *494* (3−4), 602−607.
(30) Martin-Garcia, J. M.; Luque, I.; Ruiz-Sanz, J.; Camara-Artigas, A. The promiscuous binding of the Fyn SH3 domain to a peptide from the NS5A protein. *Acta Crystallogr. D: Struct. Biol.* **2012**, *68* (8), 1030−1040.
(31) Maier, J.; Sieme, D.; Wong, L. E.; Dar, F.; Wienands, J.; Becker, S.; Griesinger, C. Quantitative description of the phase separation behavior of the multivalent SLP65-CIN85 complex. *bioRxiv* **2023**, 1−16 (last accessed 2023-02-08).
(32) Gallivan, J. P.; Dougherty, D. A. Cation-π interactions in structural biology. *Proc. Natl. Acad. Sci. U. S. A.* **1999**, *96* (17), 9459−9464.
(33) Corso, J.; Pan, K.-T.; Walter, R.; Doebele, C.; Mohr, S.; Bohnenberger, H.; Ströbel, P.; Lenz, C.; Slabicki, M.; Hüllein, J.; Comoglio, F.; Rieger, M. A.; Zenz, T.; Wienands, J.; Engelke, M.; Serve, H.; Urlaub, H.; Oellerich, T. Elucidation of tonic and activated B-cell receptor signaling in Burkitt's lymphoma provides insights into regulation of cell survival. *Proc. Natl. Acad. Sci. U. S. A.* **2016**, *113* (20), 5688−5693.
(34) Bouhaddou, M.; Memon, D.; Meyer, B.; White, K. M.; Rezelj, V. V.; Correa Marrero, M.; Polacco, B. J.; Melnyk, J. E.; Ulferts, S.; Kaake, R. M.; Batra, J.; Richards, A. L.; Stevenson, E.; Gordon, D. E.; Rojc, A.; Obernier, K.; Fabius, J. M.; Soucheray, M.; Miorin, L.; Moreno, E.; Koh, C.; Tran, Q. D.; Hardy, A.; Robinot, R.; Vallet, T.; Nilsson-Payant, B. E.; Hernandez-Armenta, C.; Dunham, A.; Weigang, S.; Knerr, J.; Modak, M.; Quintero, D.; Zhou, Y.; Dugourd, A.; Valdeolivas, A.; Patil, T.; Li, Q.; Hüttenhain, R.; Cakir, M.; Muralidharan, M.; Kim, M.; Jang, G.; Tutuncuoglu, B.; Hiatt, J.; Guo, J. Z.; Xu, J.; Bouhaddou, S.; Mathy, C. J. P.; Gaulton, A.; Manners, E. J.; Félix, E.; Shi, Y.; Goff, M.; Lim, J. K.; McBride, T.; O'Neal, M. C.; Cai, Y.; Chang, J. C. J.; Broadhurst, D. J.; Klippsten, S.; De wit, E.; Leach, A. R.; Kortemme, T.; Shoichet, B.; Ott, M.; Saez-Rodriguez, J.; tenOever, B. R.; Mullins, R. D.; Fischer, E. R.; Kochs, G.; Grosse, R.; García-Sastre, A.; Vignuzzi, M.; Johnson, J. R.; Shokat, K. M.; Swaney, D. L.; Beltrao, P.; Krogan, N. J. The Global Phosphorylation Landscape of SARS-CoV-2 Infection. *Cell* **2020**, *182* (3), 685−712 e19.
(35) Newcombe, E. A.; Delaforge, E.; Hartmann-Petersen, R.; Skriver, K.; Kragelund, B. B. How phosphorylation impacts intrinsically disordered proteins and their function. *Essays Biochem.* **2022**, *66* (7), 901−913.
(36) Heinig, M.; Frishman, D. STRIDE: a web server for secondary structure assignment from known atomic coordinates of proteins. *Nucleic Acids Res.* **2004**, *32*, W500−W502.
(37) Tamiola, K.; Mulder, F. A. A. Using NMR chemical shifts to calculate the propensity for structural order and disorder in proteins. *Biochem. Soc. Trans.* **2012**, *40* (5), 1014−1020.
(38) Shen, Y.; Bax, A. Protein backbone and sidechain torsion angles predicted from NMR chemical shifts using artificial neural networks. *J. Biomol. NMR* **2013**, *56* (3), 227−241.
(39) Lee, D.; Hilty, C.; Wider, G.; Wuthrich, K. Effective rotational correlation times of proteins from NMR relaxation interference. *J. Magn. Reson.* **2006**, *178* (1), 72−76.
(40) Dimasi, N. Crystal structure of the C-terminal SH3 domain of the adaptor protein GADS in complex with SLP-76 motif peptide reveals a unique SH3-SH3 interaction. *Int. J. Biochem. Cell Biol.* **2007**, *39* (1), 109−123.
(41) Kaneko, T.; Kumasaka, T.; Ganbe, T.; Sato, T.; Miyazawa, K.; Kitamura, N.; Tanaka, N. Structural Insight into Modest Binding of a Non-PXXP Ligand to the Signal Transducing Adaptor Molecule-2 Src Homology 3 Domain. *J. Biol. Chem.* **2003**, *278* (48), 48162−48168.
(42) Liu, Q.; Berry, D.; Nash, P.; Pawson, T.; McGlade, C. J.; Li, S. S. Structural basis for specific binding of the Gads SH3 domain to an RxxK motif-containing SLP-76 peptide: a novel mode of peptide recognition. *Mol. Cell* **2003**, *11* (2), 471−481.
(43) Farrow, N. A.; Zhang, O.; Forman-Kay, J. D.; Kay, L. E. Characterization of the Backbone Dynamics of Folded and Denatured States of an SH3 Domain. *Biochemistry* **1997**, *36* (9), 2390−2402.
(44) Bae, S.-H.; Dyson, H. J.; Wright, P. E. Prediction of the Rotational Tumbling Time for Proteins with Disordered Segments. *J. Am. Chem. Soc.* **2009**, *131* (19), 6814−6821.
(45) Rezaei-Ghaleh, N.; Klama, F.; Munari, F.; Zweckstetter, M. Predicting the Rotational Tumbling of Dynamic Multidomain Proteins and Supramolecular Complexes. *Angew. Chem., Int. Ed.* **2013**, *52* (43), 11410−11414.
(46) Karunanithy, G.; Reinstein, J.; Hansen, D. F. Multiquantum Chemical Exchange Saturation Transfer NMR to Quantify Symmetrical Exchange: Application to Rotational Dynamics of the Guanidinium Group in Arginine Side Chains. *J. Phys. Chem. Lett.* **2020**, *11* (14), 5649−5654.
(47) Vemulapalli, S. P. B.; Becker, S.; Griesinger, C.; Rezaei-Ghaleh, N. Combined High-Pressure and Multiquantum NMR and Molecular Simulation Propose a Role for N-Terminal Salt Bridges in Amyloid-Beta. *J. Phys. Chem. Lett.* **2021**, *12* (40), 9933−9939.
(48) Sörensen, C. S.; Kjaergaard, M. Effective concentrations enforced by intrinsically disordered linkers are governed by polymer physics. *Proc. Natl. Acad. Sci. U. S. A.* **2019**, *116* (46), 23124−23131.
(49) Kjaergaard, M. Estimation of Effective Concentrations Enforced by Complex Linker Architectures from Conformational Ensembles. *Biochemistry* **2022**, *61* (3), 171−182.
(50) Honorato, R. V.; Koukos, P. I.; Jiménez-Garcia, B.; Tsaregorodtsev, A.; Verlato, M.; Giachetti, A.; Rosato, A.; Bonvin, A. M. J. J. Structural Biology in the Clouds: The WeNMR-EOSC Ecosystem. *Front. Mol. Biosci.* **2021**, *8*, 729513.
(51) van Zundert, G. C. P.; Rodrigues, J. P. G. L. M.; Trellet, M.; Schmitz, C.; Kastritis, P. L.; Karaca, E.; Melquiond, A. S. J.; van Dijk, M.; de Vries, S. J.; Bonvin, A. M. J. J. The HADDOCK2.2 Web

https://doi.org/10.1021/jacs.3c09586
J. Am. Chem. Soc. XXXX, XXX, XXX−XXX

Server: User-Friendly Integrative Modeling of Biomolecular Complexes. *J. Mol. Biol.* **2016**, *428* (4), 720−725.
(52) Kjaergaard, M.; Glavina, J.; Chemes, L. B.; Merkx, M. Chapter Six - Predicting the effect of disordered linkers on effective concentrations and avidity with the "Ceff calculator" app. *Methods Enzymol.* **2021**, *647*, 145−171.
(53) Mittal, A.; Holehouse, A. S.; Cohan, M. C.; Pappu, R. V. Sequence-to-Conformation Relationships of Disordered Regions Tethered to Folded Domains of Proteins. *J. Mol. Biol.* **2018**, *430* (16), 2403−2421.
(54) Hoh, J. H. Functional protein domains from the thermally driven motion of polypeptide chains: a proposal. *Proteins* **1998**, *32* (2), 223−228.
(55) Santner, A. A.; Croy, C. H.; Vasanwala, F. H.; Uversky, V. N.; Van, Y.-Y. J.; Dunker, A. K. Sweeping Away Protein Aggregation with Entropic Bristles: Intrinsically Disordered Protein Fusions Enhance Soluble Expression. *Biochemistry* **2012**, *51* (37), 7250−7262.
(56) Uversky, V. N. The most important thing is the tail: Multitudinous functionalities of intrinsically disordered protein termini. *FEBS Lett.* **2013**, *587* (13), 1891−1901.
(57) Huang, Q.; Li, M.; Lai, L.; Liu, Z. Allostery of multidomain proteins with disordered linkers. *Curr. Opin. Struct. Biol.* **2020**, *62*, 175−182.
(58) Horst, R.; Horwich, A. L.; Wüthrich, K. Translational Diffusion of Macromolecular Assemblies Measured Using Transverse-Relaxation-Optimized Pulsed Field Gradient NMR. *J. Am. Chem. Soc.* **2011**, *133* (41), 16354−16357.
(59) Rezaei-Ghaleh, N.; Munari, F.; Becker, S.; Assfalg, M.; Griesinger, C. A facile oxygen-17 NMR method to determine effective viscosity in dilute, molecularly crowded and confined aqueous media. *Chem. Commun.* **2019**, *55* (82), 12404−12407.
(60) Nawrocki, G.; Wang, P.-h.; Yu, I.; Sugita, Y.; Feig, M. Slow-Down in Diffusion in Crowded Protein Solutions Correlates with Transient Cluster Formation. *J. Phys. Chem. B* **2017**, *121* (49), 11072−11084.
(61) von Bülow, S.; Siggel, M.; Linke, M.; Hummer, G. Dynamic cluster formation determines viscosity and diffusion in dense protein solutions. *Proc. Natl. Acad. Sci. U. S. A.* **2019**, *116* (20), 9843−9852.
(62) Rolland, D.; Basrur, V.; Conlon, K.; Wolfe, T.; Fermin, D.; Nesvizhskii, A. I.; Lim, M. S.; Elenitoba-Johnson, K. S. J. Global Phosphoproteomic Profiling Reveals Distinct Signatures in B-Cell Non-Hodgkin Lymphomas. *Am. J. Pathol.* **2014**, *184* (5), 1331−1342.
(63) Keller, B.; Shoukier, M.; Schulz, K.; Bhatt, A.; Heine, I.; Strohmeier, V.; Speckmann, C.; Engels, N.; Warnatz, K.; Wienands, J. Germline deletion of CIN85 in humans with X chromosome-linked antibody deficiency. *J. Exp. Med.* **2018**, *215* (5), 1327−1336.
(64) Jumaa, H.; Mitterer, M.; Reth, M.; Nielsen, P. J. The absence of SLP65 and Btk blocks B cell development at the preB cell receptor-positive stage. *Eur. J. Immunol.* **2001**, *31* (7), 2164−2169.
(65) Takeuchi, K.; Sun, Z.-Y. J.; Park, S.; Wagner, G. Autoinhibitory Interaction in the Multidomain Adaptor Protein Nck: Possible Roles in Improving Specificity and Functional Diversity. *Biochemistry* **2010**, *49* (27), 5634−5641.
(66) Yuzawa, S.; Suzuki, N. N.; Fujioka, Y.; Ogura, K.; Sumimoto, H.; Inagaki, F. A molecular mechanism for autoinhibition of the tandem SH3 domains of p47phox, the regulatory subunit of the phagocyte NADPH oxidase. *Genes Cells* **2004**, *9* (5), 443−456.
(67) Havrylov, S.; Rzhepetskyy, Y.; Malinowska, A.; Drobot, L.; Redowicz, M. J. Proteins recruited by SH3 domains of Ruk/CIN85 adaptor identified by LC-MS/MS. *Proteome Sci.* **2009**, *7* (1), 21.
(68) Ababou, A.; Pfuhl, M.; Ladbury, J. E. Novel insights into the mechanisms of CIN85 SH3 domains binding to Cbl proteins: solution-based investigations and in vivo implications. *J. Mol. Biol.* **2009**, *387* (5), 1120−1136.
(69) Myers, D. R.; Zikherman, J.; Roose, J. P. Tonic Signals: Why Do Lymphocytes Bother? *Trends Immunol.* **2017**, *38* (11), 844−857.

https://doi.org/10.1021/jacs.3c09586
J. Am. Chem. Soc. XXXX, XXX, XXX−XXX